Oceanic nutrient and oxygen transports and bounds on export production during the World Ocean Circulation Experiment

Alexandre Ganachaud[1]

Institut de Recherche pour le Développement, Laboratoire d'Etudes Géophysiques et d'Océanographie Spatiale, Toulouse, France

Carl Wunsch

Massachusetts Institute of Technology, Cambridge, Massachusetts, USA

Received 31 July 2000; revised 4 September 2001; accepted 2 November 2001; published 16 October 2002.

[1] Large-scale oceanic transports of nutrient and oxygen are estimated from selected hydrographic sections from the World Ocean Circulation Experiment spanning the world ocean. A so-called geostrophic inverse box model is used to calculate the velocity field across the transoceanic sections. The circulation is required, a priori, to conserve mass, salt, top-to-bottom silicate, and subsurface heat and PO(= 170P + O_2). The resulting estimate of the time mean circulation is used to compute horizontal and vertical nutrient transports and their residual sources and sinks associated with biogeochemical processes. Locally, the remineralization rate is, in general, below our uncertainty level, with magnitudes consistent with in situ measurements (0 ± 0.1mol N m^{-2} yr^{-1} to 0.7 ± 0.25 mol N m^{-2} yr^{-1} below about 100 m). Because of correlations between errors, the export production becomes significant when integrated globally, with 390 ± 240 kmol Si s^{-1} and 57 ± 40 kmol N s^{-1}(420 ± 290 kmol C s^{-1}) between 47°N and 30°S and at 2000 m. Examination of N* provides estimates for nitrate fixation and denitrification, either consistent (North Atlantic) or contradictory (Indian) with previous findings. Similarily, oxygen utilization rates and net air-sea exchanges are provided. A net uptake of oxygen at high latitudes and an outgassing at low latitudes are found. Examination of the pseudotracer O* suggests an important role of dissolved organic matter in the oxygen budget. Oceanic oxygen and O* are found in global balance within uncertainties. *INDEX TERMS:* 4805 Oceanography: Biological and Chemical: Biogeochemical cycles (1615); 4203 Oceanography: General: Analytical modeling; 4845 Oceanography: Biological and Chemical: Nutrients and nutrient cycling; 4863 Oceanography: Biological and Chemical: Sedimentation; *KEYWORDS:* export production, nutrient cycles, oxygen cycle, biogeochemical cycles

Citation: Ganachaud, A., and C. Wunsch, Oceanic nutrient and oxygen transports and bounds on export production during the World Ocean Circulation Experiment, *Global Biogeochem. Cycles*, *16*(4), 1057, doi:10.1029/2000GB001333, 2002.

1. Introduction

[2] Through its ability to transport energy, freshwater, oxygen, and nutrients among other properties, and to transfer them to and from the atmosphere, the ocean plays a major role in climate regulation. One of the main objectives of the World Ocean Circulation Experiment (WOCE) was the quantitative determination of such transports.

[3] Oceanic carbon exchanges with the atmosphere and interior transports are important additional properties of intense climate interest. A large fraction of the carbon fixed in the oceanic surface waters is recycled in the euphotic zone, with the balance exported towards the deep ocean. This export is believed to control and regulate air-sea CO_2 exchanges, but few methods exist to estimate its rate. Satellite measurements of ocean color provide an estimate of the biomass in the upper layers [e.g., *Antoine et al.*, 1996], from which the primary production can be calculated. Such satellite-derived primary production estimates are very uncertain, as is their relationship to export production, being controlled by factors including temperature, the food-web structure or the particle aggregation [*Laws et al.*, 2000; *Aufdenkampe et al.*, 2001]. Export production varies greatly with time, approaching 50–80% of the primary production during episodic blooms or in high productivity areas, but normally is about 5–10% of primary production [*Buesseler*, 1998].

[4] *Lampitt and Antia* [1997] reviewed the existing particle flux measurements from deep sediment traps. Using their normalization function,

[1]Now at Institut de Recherche pour le Developpement, Centre de Noumea, Noumea, New Caledonia.

0886-6236/02/2000GB001333$12.00

$$J(z_1) = J(z_0) \times \left(\frac{z_0}{z_1}\right)^{0.858}, \quad (1)$$

where J is the downward flux of organic matter, z_0 the depth of measurement, and z_1 the depth of interest, we extrapolated the annual-average export production at z_1 = 150 m. In all oceanic regions excluding the polar oceans, it ranges from 0.04 to 0.4 mol N m^{-2} yr^{-1} (here and in the following, all production numbers are given in nitrate units, assuming a N/C ratio of 16/117 [*Anderson and Sarmiento*, 1994]). Because function (1) is an approximation, the extrapolated values at 150 m are much more uncertain than the values at 2000 m (K. Buesseler, personal communication, 1999). In polar regions, the variations are more extreme, with values reported between 0.01 and 0.7 mol N m^{-2} yr^{-1}. Shallow sediment traps would be in principle be more appropriate than our extrapolation, but those results are difficult to interpret due to strong measurement biases [*Siegel and Deuser*, 1997; *Buesseler*, 1991]. Export production estimates based upon the ^{234}Th method [*Michaels et al.*, 1994; *Buesseler*, 1998] are about ten times higher than from the traps, ranging from 0.14 to 1.4 mol N m^{-2} yr^{-1} for all oceans excluding the polar regions, and from 0.04 to 4 mol N m^{-2} yr^{-1} in the latter areas.

[5] Alternatively, export production can be derived from transports of dissolved nutrients. A downward flux of particles and dissolved organic matter creates a sink of dissolved nutrients in the upper layers by consumption, and a source in the lower layers through dissolution (remineralization). As a result, the subsurface nutrient concentrations represent a time and space average of biogeochemical processes, a relatively stable integral, as measurements have shown no statistically significant variations in large-scale concentration distributions over the past several decades. In this assumed steady state, the source terms are balanced by horizontal and vertical transports. Photosynthesis and remineralization produce similar source terms in the oxygen budget, but with opposite sign. In addition, and unlike nutrients, the oceanic oxygen cycles include important air-sea fluxes.

[6] *Schlitzer* [2002] used a steady biogeochemical ocean circulation model fit to climatological tracer concentrations, and calculated a total export of 3500 kmol N s^{-1}, a figure similar to the biogeochemical numerical model of *Najjar et al.* [1992] (4400 to 5500 kmol N s^{-1}). The *Schlitzer* [2002] export production estimates exceeded satellite-derived values by up to a factor of 5 in the Southern Ocean (30% of the global export), but agreed well everywhere else.

[7] In the present paper, we lay a foundation for the eventual description of the carbon budget based on the newly available global WOCE hydrographic sections. A global ocean circulation estimate has been made [*Ganachaud*, 1999; *Ganachaud and Wunsch*, 2000] that is kinematically and dynamically self-consistent. This permits the diagnosis of nutrient and oxygen transports across sections at the high spatial resolution of WOCE hydrography. Corresponding sources and sinks (divergences) of dissolved nutrients are estimated between sections and discussed in relation to export production. After a brief summary of the model and estimation procedure, the discussion begins with the silica cycle, followed by the analysis of nitrate, phosphate and oxygen.

2. Ocean Circulation Estimate

2.1. Hydrographic Model

[8] The physical circulation estimate has been described in detail elsewhere [*Ganachaud and Wunsch*, 2000; *Ganachaud et al.*, 2000], and we only summarize the main features. Estimates are based on the selected hydrographic sections of Figure 1 from the World Ocean Circulation Experiment (WOCE) and Jakarta Australia Dynamic Experiment (JADE).

[9] Volumes of ocean bounded by these sections are divided into vertical layers defined by so-called neutral surfaces, denoted γ^n [*Jackett and McDougall*, 1997] which are equivalent to the more conventional isopycnal surfaces, with the number of layers varying with region between 11 and 19. The circulation is geostrophic with an Ekman layer at the surface. A large variety of constraint equations is written for each section and oceanic volume. These include, near-conservation of mass, salt and top-to-bottom silicate. (Justification for the last constraint is provided below). In addition, heat and the phosphate-oxygen combination "PO" ($170[PO_4] + [O_2]$) are conserved when they are not in contact with the surface. Other constraints involve horizontal transports across the sections (see *Ganachaud* [1999] and *Ganachaud and Wunsch* [2000] for details). Thus the property transports both partially determine, and are determined by, the inferred mass transports.

[10] A best estimate solution is found following now conventional inverse methods [*Wunsch*, 1996]. The result is a dynamically and kinematically consistent (within error bars) flow field (A. Ganachaud, Error budget of inverse box models: The North Atlantic, submitted to *Journal of Atmospheric and Oceanic Technology*, 2002] providing an estimate of property transports (mass, heat, salt, nutrients, oxygen) across each bounding hydrographic section, in each layer, and an estimate of the property imbalance within each layer volume. The horizontal spatial resolution of the solution is about 50 km on average in each section, which can be regarded as near-eddy resolving. This high resolution using nearly synoptic sections distinguishes the solution from those based upon smoothed (in space and time) climatologies which tend to systematically underestimate actual property transports.

[11] As with all inverse solutions, an accompanying detailed error budget permits calculation of the statistical uncertainties of quantities derived from the flow field. The solution mass transport (nominally representing 1990–1996, but a few sections are from the pre-WOCE period, 1986–1989) are not radically different from previously published estimates, as described in the references. They are consistent also, within error estimates, with the only previous global inverse solution from hydrographic lines of *Macdonald* [1998] whose data set was from an earlier time interval. For the scalar property transports of interest here, a technical change was made to previously used methods: property anomaly constraints were employed so as to reduce the errors owing to residual mass imbalances in the overall circulation.

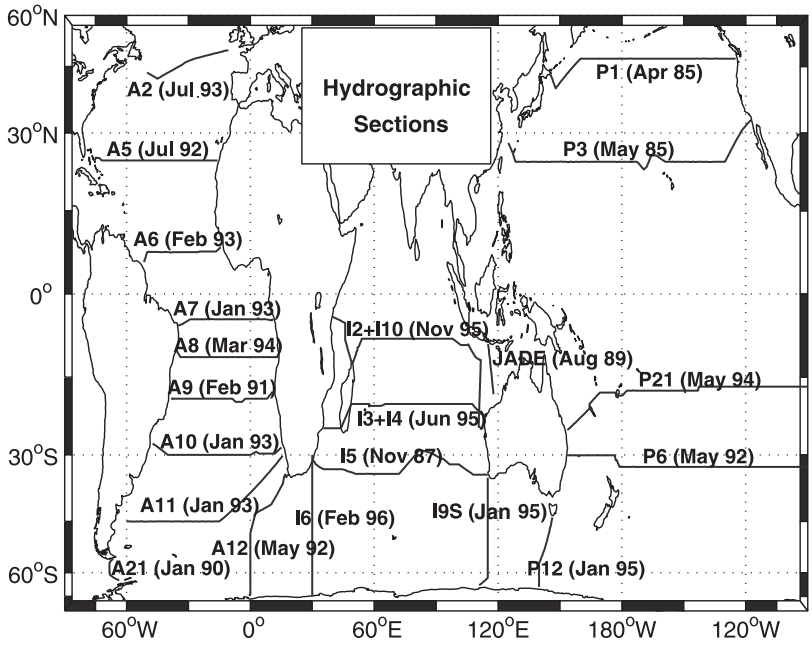

Figure 1. Hydrographic sections used in the calculation. Sections from WOCE, pre-WOCE, and JADE were selected to avoid open-ocean crossing points and to cover the period 1985–1996. The full station spatial resolution is retained.

[12] Nutrient and oxygen transports and divergences are calculated from the absolute velocity field along the sections and the vertical (dianeutral) transfers within the areas bounded by sections within layers bounded by neutral surfaces. To compute uncertainties, the full covariance matrix of the inverse model solution is used, so that the uncertainty of the circulation is accounted for, including aliasing of temporal variability in temperature and salinity. However, the uncertainty due to seasonal variations in surface nutrient concentrations is not included.

2.2. A Note on Terminology

[13] We use the terminology of fluid flow. Horizontal "transports" here are integrals of the products of absolute velocities, v, property concentrations, C, and density ρ. Vertical (interlayer) transports are similarly the product of vertical velocities, w with concentration (ρwC), plus diffusion, $\kappa\partial\rho C/\partial z$. Then by convention, the "convergence" of C over a finite volume is the sum of $\rho vC + \rho wC + \kappa\partial\rho C/\partial z$ into a closed volume such that ρv sums to zero (mass-conservation). If the sum is not zero and is positive, then there is either an internal sink, or a removal by other processes (e.g., air-sea transfer), or a noise in the calculation. If the sum is negative, one must either have an internal source, or an inward boundary flux, or noise (and negative convergences are often called the "divergence"; convergence and divergence are used interchangeably, because one is the negative of the other). A critical issue in formulating the budget of any parameter C is distinguishing the noise in the calculation from the physical processes of sources/sinks/vertical advection/boundary transports and this need is addressed at length below.

[14] We will now discuss in turn the property transfers of biogeochemical interest that are determined as part of the solution to the inverse problem.

3. Silicate Transports, Sources, Sinks, Export Production

[15] Siliceous planktonic organisms consume surface dissolved silicate to build their skeletons [e.g., *Broecker and Peng*, 1982]. Most skeletons end up dissolving in surface and deep waters, although a fraction are buried on the seafloor, mostly in highly productive areas, forming opaline bands there under upwelling areas [*Archer et al.*, 1993]. The efficiency of opal dissolution within the water column varies by orders of magnitude depending, for instance, on temperature and species [*Ragueneau et al.*, 2000]. Except in the Southern Ocean, available measurements and models suggest that siliceous shells do not dissolve substantially before they reach the seafloor [e.g., *Sayles et al.*, 1996], but understanding of this process is limited by the lack of knowledge of lateral advection, resuspension and biases in trap measurements due to strong currents [*Ragueneau et al.*, 2000]. Particles reaching the bottom remain on the seafloor for a few hundred years; most of them apparently eventually remineralize with only a small fraction fully buried and lost to the ocean system.

[16] Given the very different time scales involved in the silica cycle, and given the scarcity of sediment trap data used to describe large scale behavior, there is a large uncertainty in their description. *Ragueneau et al.* [2000] deplore a "major gap in our understanding of the mechanisms controlling the competition between retention in and export from surface waters". Not only does the opal export

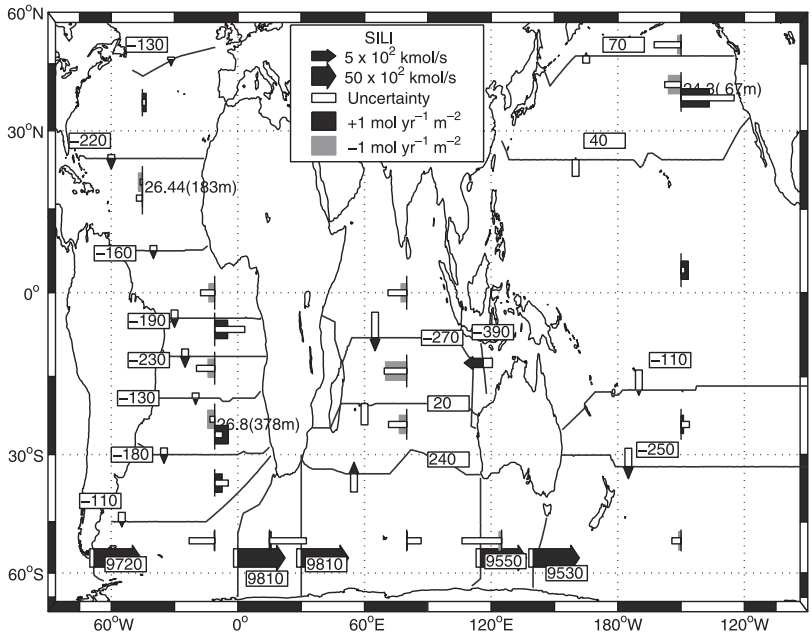

Figure 2. Global dissolved silicate transports and divergences. The length of each arrow corresponds to the silicate transports between continents. The open boxes behind each arrow indicate the uncertainty (one standard deviation). Between sections, silicate divergences are indicated by the solid boxes, either top-to-bottom (single box) or surface/deep (double box) (see text). In the latter case, the number indicates the interface (in neutral density units). Divergences are not given where the uncertainty exceeds 150% (as measured by the one standad deviation estimates).

flux vary by a factor of 100, but sediment trap measurements also can be uncertain by a factor of 10, in particular at shallow levels [e.g., *Buesseler*, 1991]. In this section, we provide evidence that silicate should be, a priori, approximatively conserved, and analyze the net sources and sinks of silicate in relation with opal dissolution.

3.1. Conservation of Top-to-Bottom Silicate

[17] Total (top-to-bottom) conservation of silicate was required in the constraints in the inverse calculations. According to *Nelson et al.* [1995], 50% of the global opal production is recycled in the euphotic zone, allowing a maximum global particle flux of 4500 kmol Si s^{-1} to enter the deep layers (these numbers are highly uncertain). Some of the particles are buried there with an average global burial/production of 3%. The burial is believed to be almost negligible in the large oligotrophic regions [e.g., *Tréguer et al.*, 1995]. In high-productivity regions such as the Southern Oceans, recent isotopic measurements from the JGOFS Antarctic program indicate that little burial has occurred for at least the last 5000 years, with a maximum of 5% of the total production (F. Sayles, personal communication, 2001). This result contradicts previous beliefs that up to 25% of the total production was buried there [*DeMaster et al.*, 1991].

[18] Net sources and sinks of silicate thus appear to be much smaller than biogenic fluxes. The global sink of silicate estimated from sediment data is about 220 kmol Si s^{-1}, which is close to the total input from river runoff, at 160 kmol Si s^{-1} [*Tréguer et al.*, 1995]. Other sources of silica, such as hydrothermal activity, basaltic erosion and eolian inputs, are estimated as 40 kmol Si s^{-1} in total [*Tréguer et al.*, 1995] although little is known about them.

[19] To first order therefore the fluxes of silica are essentially a vertical balance between export and deep or bottom remineralization in the water column. When diagnosed within a top-to-bottom oceanic volume enclosed by hydrographic sections, silicate is expected to be nearly conservative, as in our imposed constraint. Nonconservation can occur for a variety of reasons, including the erosion of the seafloor during a transient event; time changes in export production; and the horizontal advective transport of siliceous particles. A more complete analysis is described by *Ganachaud* [2002], who estimated that the size of these processes is relatively small, in the North Atlantic, compared to the a priori uncertainties in silicate transports. The *Ganachaud* [2002] North Atlantic a priori silica uncertainties were extended to the global ocean as explained in Appendix A.

3.2. Analysis of Sources and Sinks of Dissolved Silicate

[20] Estimated sources and sinks of silicate, i.e., convergences and divergences of advective and vertical diffusive transports, were examined in each oceanic region delimited by the sections of Figure 1 and within each oceanic layer. (At the high resolution of hydrographic sections, horizontal diffusive tranports are assumed to be much smaller.) Figure 2 shows the silicate transports (vectors) and divergences (bars within boxes). Numerical values for the transports and divergences are tabulated in Appendix 6.

[21] Horizontal silicate transports (arrows) are directed southward within the Atlantic Ocean with -150 ± 75 kmol Si s^{-1}; eastward in the Southern Ocean, and are indistin-

guishable from zero in other regions. Most divergences in individual layers were found to be less than one standard deviation of their uncertainty, and consequently formally indistinguishable from zero. However, when a sign change occurs between the surface and the subsurface layers, the divergences were summed separately over near-surface and deep layers. The separating neutral surfaces and their average depth are indicated on Figure 2. Because the depth of neutral surfaces varies with location, this choice of separation (surface/deep) does not correspond to a given depth, such as the bottom of the euphotic zone. In boxes where divergences within individual layers were more than 150% uncertain, the summation was done over all layers (top-to-bottom).

[22] Consistent with the imposed conservation constraint, top-to-bottom silicate divergences are indistinguishable from zero almost everywhere. An exception occurs in the central Pacific Ocean where the divergences differs from zero at near two standard errors, indicating potential failure there of the hypothesis of local silicate balance. This large-scale imbalance is directly related to the large Pacific-Indonesian Throughflow (hereafter ITF) in the solution, here estimated at $15 \pm 6 \times 10^9$ kg s^{-1} [*Ganachaud et al.*, 2000], consistent with the most recent measurements in the Makassar Strait [*Gordon et al.*, 1999]. The issue is whether the associated silicate transport in the ITF (400 ± 300 kmol Si s^{-1} to the west) is representative of the time-average transports. Only one JADE section with nutrient measurements was available for the estimate in this extremely time-variable region. Our ITF estimate implies a silicate source in the Pacific Ocean (+0.35 ± 0.15 mol SiO_2 yr^{-1}m^{-2}) exporting to the Indian Ocean with a corresponding sink there of (−0.28 ± 0.24 mol SiO_2 yr^{-1}m^{-2}) that may well derive from a seasonal alias, and which should not be taken very seriously at this time.

[23] In the Southern Ocean we find a net, uncertain sink of dissolved silicate at −480 ± 380 kmol Si s^{-1} (equivalent to −0.18 ± 0.15 mol SiO_2 yr^{-1}m^{-2} overall). The Southern Ocean is indeed the main region of silica sedimentation, with largest accumulation between 0.36 and 1.24 mol SiO_2 yr^{-1}m^{-2} in "focusing" regions and low values of 0.007 mol Si m^{-2} yr^{-1} in the Ross Sea (Table 3) [e.g., *Ragueneau et al.*, 2000]. Our total average convergence of 0.18 mol SiO_2 yr^{-1}m^{-2} seems comparatively large, although in situ measurements are too scarce to estimate an average. Because most layers are in contact with the surface, we cannot determine at what depth the sink occurs, and thus are not able to identify a particular process.

3.3. Relation to Export Production

[24] In most temperate regions, a sink of silicate exists in the upper layers, with values ranging from −0.1 ± 0.05 to −1 ± 0.6 mol SiO_2 yr^{-1}m^{-2}; a corresponding source exists in the underlying deep layers (Figure 2). Although highly uncertain, this structure corresponds to what one expects from the large-scale average biological consumption of silicate and opal dissolution.

[25] The relation between the diagnosed divergences of silicate and sediment trap measurements is not straightforward. Sources in the deep layers of our model are integrated below a neutral surface whose depth necessarily varies with time and location between the surface and about 380 m (away from the Southern Ocean). As a result, remineralization and consumption are integrated in space and time. The inferred source term therefore corresponds to the quantity of nutrient that is effectively entrained in the deep oceanic circulation and removed from the surface on relatively long timescales, in contrast to sediment trap measurements (and the classical definition of primary production) that give a net flux of organic matter across a fixed depth. Only qualitative comparison with sediment trap results is therefore possible. Opal rains are indeed in the same range of 0.05 to 1.3 mol SiO_2 yr^{-1}m^{-2}, excluding polar oceans where the range is larger, *Lampitt and Antia*'s [1997] Table 2, normalized at 150 m.

Table 1. Large-Scale Integrals of Opal Dissolution (kmol Si s^{-1})

Region	Si Source Below[a]		
	2000 m	1000 m	Surface[b,c]
30°S–47°N	390 ± 240	470 ± 390	600
ATL[d]	−40 ± 90	70 ± 100	20 ± 120
IP[e]	430 ± 220	400 ± 370	580
TROP[f]	3 ± 190	200 ± 330	140
SUBP[g]	387 ± 240	270 ± 330	460 ± 800

[a] Below neutral surfaces corresponding approximately to 2000, 1000, and 100 m.
[b] The first layer neutral surface is γ^n = 26.44 kg m^{-3} (North Atlantic); 26.2 (South Atlantic); 24.3 (Pacific) and 25 (Indian), with depths varying strongly with location, around 100 m.
[c] The surface layers were not constrained in the central Pacific because of the Indonesian Throughflow, resulting in a very large formal uncertainty in layers above 1000 m. We do not report those uncertainties.
[d] Atlantic, 30°S–47°N.
[e] Indian + Pacific, 30°S–47°N.
[f] Tropical: 20°S–24°N.
[g] Subpolar: 30°S–20°S + 24°N–47°N.

[26] Because errors are globally correlated in the hydrographic model, uncertainties tend to decrease when integrated on large scales (this reduction need not occur generally). Table 1 gives integrated sources and sinks for latitude bands and below neutral surfaces at approximately 2000, 1000 and 100 dbar. The resulting divergences correspond to the net export production, as we just defined it, below that depth. The net silica dissolution below 2000 m and between 47°N and 30°S is of 390 ± 240 kmol Si s^{-1} (or an average rate of 0.05 ± 0.03 mol Si m^{-2} yr^{-1}), comparable with *Lampitt and Antia* [1997] (0.006 to 0.1 mol Si m^{-2} yr^{-1}). Using existing ^{14}C production estimates combined with silica/carbon ratio in siliceous organisms, *Tréguer et al.* [1995] estimated an upper bound of 9000 kmol Si s^{-1} for the global primary production of siliceous organisms. Their lower bound estimate, 6400 kmol Si s^{-1}, was obtained from a model. Normalized to 2000 m using (1), the value would range from 640 to 900 kmol Si s^{-1}, comparable with our number (including the Souther Ocean sink). Table 1 also suggests that away from the Southern Ocean, silica dissolution occurs essentially in the temperate latitudes of the Indian and Pacific oceans.

4. Nitrate and Phosphate

[27] Figures 3 and 4 show the dissolved nitrate and phosphate net transports and divergences. As for silicate,

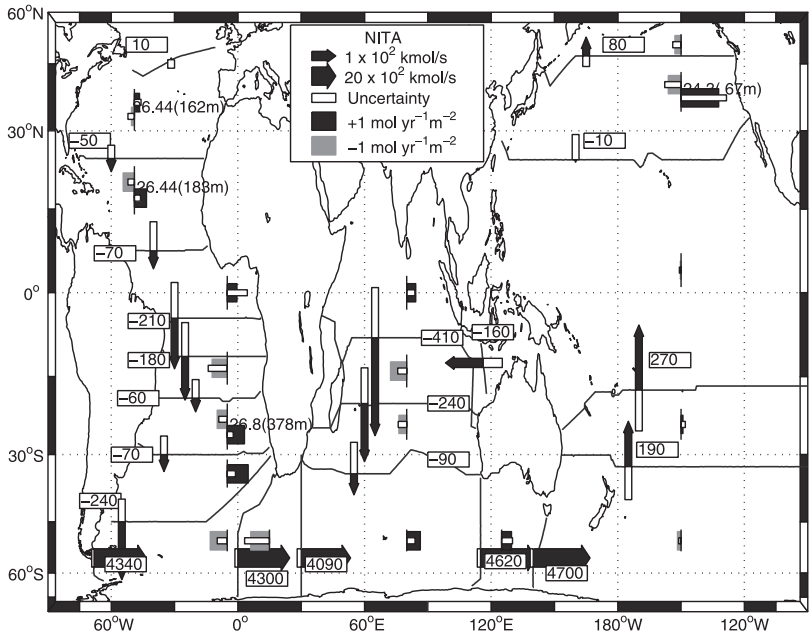

Figure 3. Same as Figure 2 but for dissolved nitrate.

divergences of dissolved inorganic nutrients in oceanic layers were summed, either top-to-bottom (single shaded bars) or within surface and deep layers if there was a systematic sign change with depth. There is an indication of southward nitrate transport from the Atlantic Ocean at 45°S (A11, i.e., a net nitrate divergence of 340 ± 120 kmol N s^{-1} between 48°N and 45°S in the Atlantic) as well as phosphate (16 ± 8 kmol P s^{-1}). Seventy percent of the corresponding nutrient regeneration occurs in the South Atlantic between 30°S and 45°S. North of 45°S, the uncertainty of net nitrate transports is close to 100%, while in the Southern, South Pacific and Indian oceans, net transports are significant, associated with the net mass transport.

[28] The divergences show that in the north tropical and south subtropical (19°S–30°S) Atlantic boxes, shallow nutrients are depleted with a source in the deep layers (Figure 3), with the separating depth at about 180 m. A similar feature is present in the Central and North Pacific and both may correspond to a net average vertical particle flux associated with consumption and remineralization. In the rest of the ocean, the divergences were too uncertain to make this distinction. Net (top-to-bottom) sources or sinks

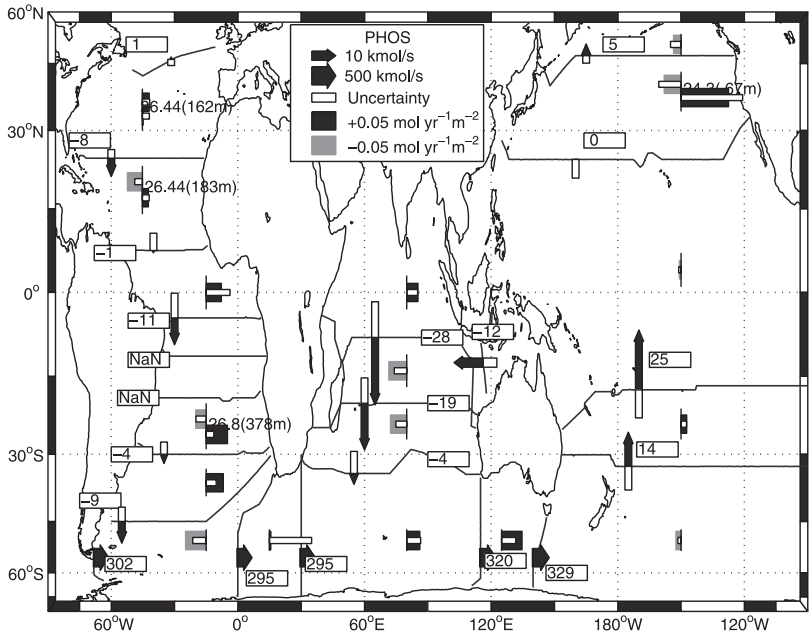

Figure 4. Same as Figure 2 but for dissolved phosphate.

of nitrate and phosphate are found in several oceanic regions, notably in the North Atlantic (0.1 ± 0.1 mol N $m^{-2}yr^{-1}$). Such a source was also found by *Rintoul and Wunsch* [1991] using older data, between 24°N and 36°N (versus 24°N and 48°N here).

[29] In deep layers, net sources of nitrate range from 0.5 ± 0.24 mol N $m^{-2}yr^{-1}$ (tropical North Atlantic) to 0.7 ± 0.2 mol N $m^{-2}yr^{-1}$ (South Atlantic), comparable with our extrapolation from deep moored sediment traps (0.04 to 0.4 mol N $m^{-2}yr^{-1}$) [*Lampitt and Antia*, 1997]. Export production estimates from isotopic measurements in temperate and tropical oceanic region also range from 0.05–1.4 mol N $m^{-2}yr^{-1}$ [*Buesseler*, 1998]. New production estimates are in the same range, with about 0.5 mol N $m^{-2}yr^{-1}$ [e.g., *Jenkins and Goldman*, 1985], in agreement with the nutrient sinks found in the surface layers in the Atlantic, namely, −0.4 ± 0.3 mol N $m^{-2}yr^{-1}$ in the South Atlantic and −0.5 ± 0.25 mol N $m^{-2}yr^{-1}$ in the tropical North Atlantic. (New production is defined here as the amount arising from the nutrient supply derived from the deep layers in a hypothetical one-dimensional balance. In the absence of horizontal advection, new production is equivalent to export production.) Magnitudes of the estimated nitrate divergences are in close agreement with independent inferences despite the different approach that we use (see previous section). Overall, nitrate sources (including deep/surface and net in a box) are in the range −0.8 ± 1 mol N $m^{-2}yr^{-1}$ to −1.8 ± 1.8 mol N $m^{-2}yr^{-1}$.

[30] When summed globally, nitrate export is significant (Table 2), with a total of 57 ± 40 kmol N s^{-1} (0.008 ± 0.006 mol N m^{-2} yr^{-1}) at 2000 m between 30°S and 47°N; and 440 kmol N s^{-1} (0.06 mol N m^{-2} yr^{-1}) below the first model layer (the latter number being highly uncertain). Such export is comparable with the compilation of *Lampitt and Antia* [1997] (0.004 to 0.04 mol N m^{-2} yr^{-1} at 2000 m and 0.04 to 0.4 mol N m^{-2} yr^{-1} normalized at 150 m). The statistically most significant numbers, at 1000 m, indicate twice as much nitrate export in the tropical band as in the temperate regions, with no dominance of a particular ocean, in contrast to the silicate results.

[31] Net nitrate and phosphate convergences (divergences) were integrated over latitude bands (Table 3). Similar features are seen in both fields, with about 100% uncertainty. High latitude oceans are nitrate and phosphate sources, while the tropical band is a sink. These inferred sources and sinks may also be the result of advection of dissolved organic matter [*Rintoul and Wunsch*, 1991; *Najjar et al.*, 1992], and/or temporal aliasing of the nutrient transports across the sections, but all are formally indistinguishable from zero. Both dissolved nitrate and phosphate are balanced globally.

Table 2. Same as Table 1 but for Nitrate Remineralization (kmol N s^{-1})

	N Source Below		
Region	2000 m	1000 m	Surface
30°S–47°N	57 ± 40	170 ± 80	440
ATL	4 ± 25	90 ± 40	140 ± 150
IP	53 ± 30	80 ± 70	300
TROP	0 ± 30	120 ± 70	30
SUBP	57 ± 40	50 ± 70	410 ± 660

Table 3. Nitrate and Phosphate Sources and Sinks Integrated Globally Over Latitude Bands (kmol s^{-1})

Latitude	Nitrate	Phosphate
24°N–48°N	100 ± 110	10 ± 8
30°S–24°N	−90 ± 200	−13 ± 13
South of 30°S	100 ± 250	10 ± 15
Global total[a]	40 ± 300	−3 ± 20

[a] The global total includes the northern part (north of 48°N).

[32] In general, phosphate divergences are similar to those for nitrate (Figures 3 and 4). Two possibilities for explaining the divergences are again, (1) the advection of dissolved organic matter and, (2) an error due to aliasing of the seasonal cycle in the hydrographic sections (most measurements are from the summer). To identify sources that are specific to nitrate, we calculated the so-called N* transports and divergences [*Gruber and Sarmiento*, 1997]. The subtropical North Atlantic exhibits a net loss of N*, implying denitrification (Figure 5), while the tropical Atlantic has net N-fixation.

[33] The total (subtropical + tropical) is an uncertain source of 30 ± 37 kmol N s^{-1}, or 0.070 ± 0.09mol N m^{-2} yr^{-1}, interestingly equal to the *Gruber and Sarmiento* [1997] estimate in this region (0.072 mol N m^{-2} yr^{-1}). Net N-fixation is also found in the subtropical South Atlantic (87 ± 38 kmol N s^{-1}, or 0.4 ± 0.17mol N m^{-2} yr^{-1}). In the Indian Ocean, we find net fixation in the subtropical region, net denitrification in the south tropical region and no significant value in the North Indian Ocean–a region of known denitrification. On the whole, the Indian Ocean is fixing nitrate (51 ± 48 kmol N s^{-1}), in contradiction to *Gruber and Sarmiento* [1997] who suggest net denitrification from the two GEOSECS sections. In the Pacific Ocean, N* is in balance, with denitrification in the south subtropical Pacific cancelling nitrate fixation to the North. Because nitrate fixation and denitrification occur at the same latitudes (*Deutsch et al.* [2001] describe the contrast between east and west Pacific along the same latitudes), our zonal averages do not capture the main signals, rendering difficult the comparison with existing estimates.

5. Oxygen

[34] The amount of oxygen that is pumped into, or outgassed by, the ocean depends upon the partial pressure. In the ocean, partial pressure is controlled by (1) temperature and, to a minor extent, salinity [e.g., *Garcia and Gordon*, 1992] (“solubility pump”); (2) biological production and respiration (“biological pump”); and locally (3) oceanic transport and upwelling. At saturation, an increase in temperature implies a release of oxygen to the atmosphere and vice versa through (1) [*Stephens et al.*, 1998]. The three mechanisms can reinforce or cancel. For instance in subtropical gyres, warming, productivity and advection create an outgassing, while at high latitudes cooling and convection both imply an oxygen uptake.

5.1. Oxygen Transports and Divergences

[35] Figure 6 shows the net transports and divergences of dissolved oxygen from the ocean circulation estimate. In

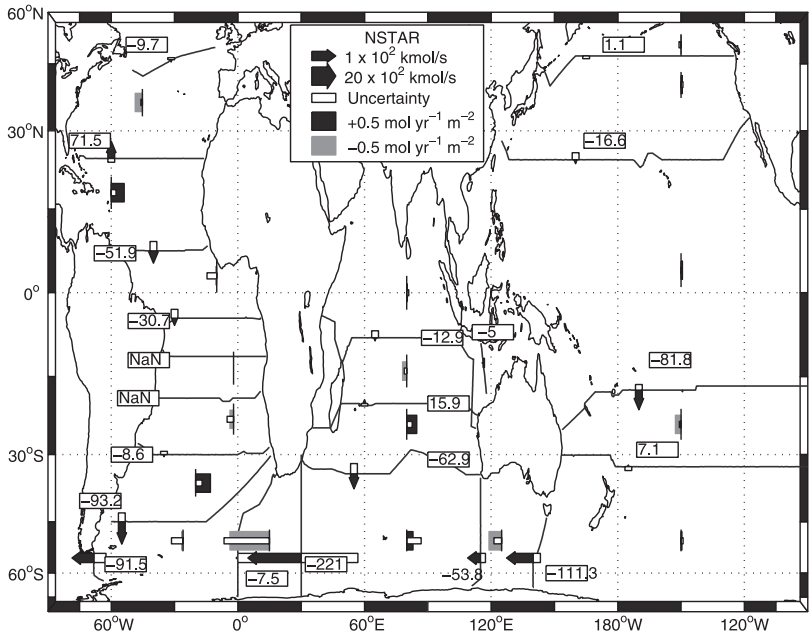

Figure 5. Same as Figure 2 but for N*. Note the change of scale for residuals, in comparison with Figure 3.

contrast with nutrients, the figures differ significantly from zero in many places. A large source (uptake and photosynthesis) of oxygen is observed in polar and temperate regions, with a loss in the tropics. Oxygen transports are directed equatorward almost everywhere, except in the southern Indian Ocean because of the southward oxygen transport there associated with the incoming ITF. Locally, net loss of oxygen reaches values of up to 8 ± 1 mol O_2 $m^{-2}yr^{-1}$ in the South Atlantic. In this particular region, the oxygen loss occurs over the first 1000 dbars, consistent with remineralization. In the North Atlantic, South Atlantic and North Pacific temperate regions, distinctive regimes can be identified in surface and deep layers, with an oxygen gain in the surface layers, associated with atmospheric uptake and,

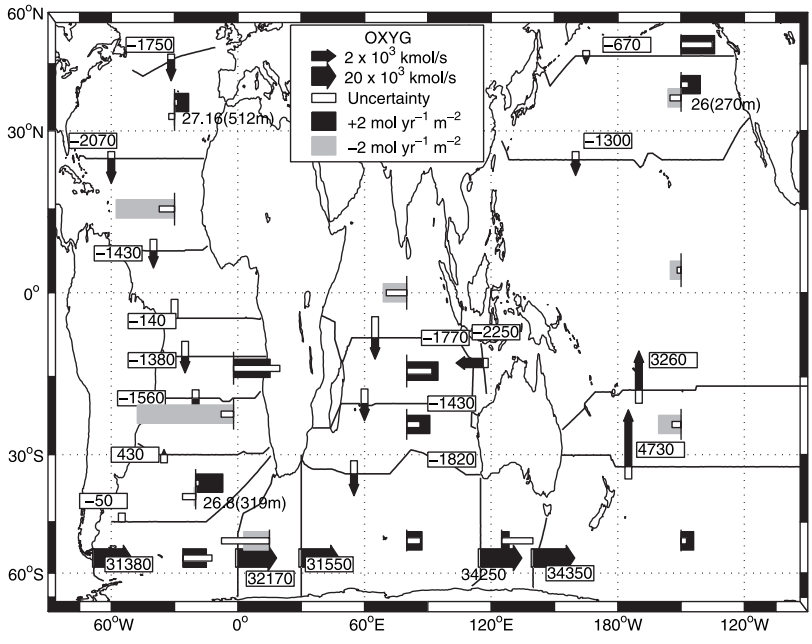

Figure 6. Dissolved oxygen transports and divergences as for nutrients (Figure 2), i.e., divergences were summed individually in deep/shallow layers when the distinction was possible, top-to-bottom otherwise.

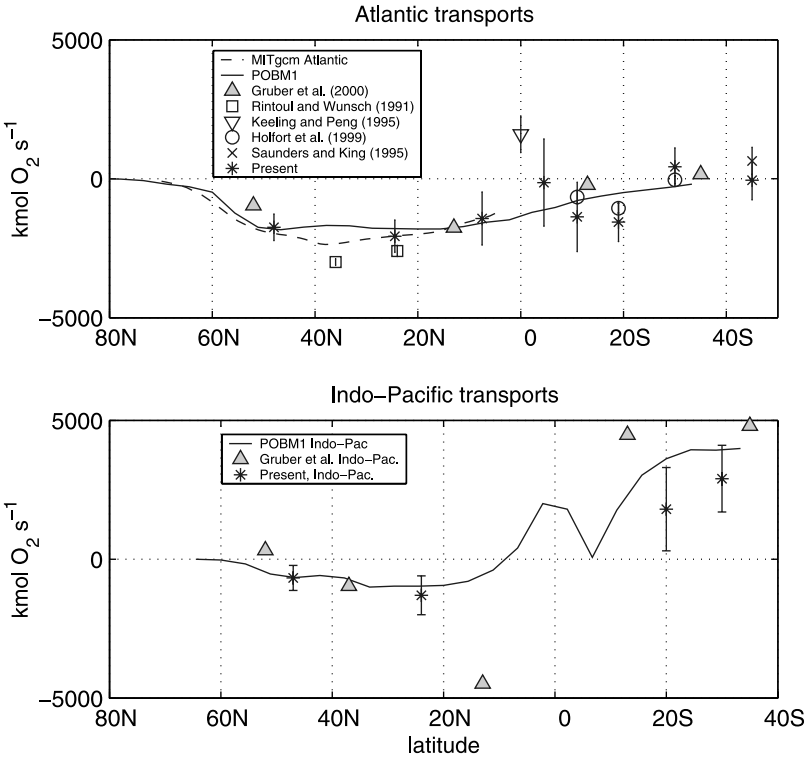

Figure 7. Atlantic and Indo-Pacific dissolved oxygen transports (stars). MITgcm = MIT General Circulation Model (offline biogeochemical code; [e.g., *Mckinley et al.*, 2000]); POBM1 = Princeton Ocean Biogeochemistry Model Version 1 [e.g., *Stephens et al.*, 1998].

possibly, a contribution from photosynthesis. In the deeper layers, an uncertain loss is found, one presumably owing to remineralization. In layers with oxygen gain, there is no correlation with nutrient loss and the biological pump is probably masked by the solubility pump. Oxygen utilization is correlated with nutrient input at depth (for instance, in the South Atlantic, 19°S–30°S).

[36] The Atlantic and Indo-Pacific transports are compared with other results in Figure 7. There is an overall agreement within one standard deviation, of our results, except for the *Keeling and Peng* [1995] estimate which is directed to the north at the equator. The agreement in both regions between the various estimates, the MIT general circulation (GCM) off-line model [*McKinley et al.*, 2000], as well as the Princeton Ocean Biogeochemistry Model [*Stephens et al.*, 1998] is remarkable (and probably fortuitous, given the uncertainties). The *Gruber et al.* [2001] estimate was derived from an integration of air-sea oxygen fluxes, themselves estimated through a combination of WOCE hydrographic observations and transport functions obtained from a GCM. Their results suggest, as do ours, a net southward transport in the Atlantic, north of 30° S and equatorward transports in the Indo-Pacific Basins. As they point out [*Gruber et al.*, 2001, Figure 7], their South Indo-Pacific transport (their experiment labeled SIL(u)) is slightly larger than ours, possibly due to an overestimate of the equatorial outgassing in the OGCM.

[37] To separate the effects of biology and solubility, we computed the divergences of $O^* = O_2 + 170PO_4$ [*Gruber et al.*, 2001], which is supposed to reflect air-sea exchanges alone (Figure 8). In the Atlantic and in the central Pacific, O* divergences are 50% or more higher than O_2 divergences. The difference derives from the net phosphate divergences (Figure 4), associated with horizontal transports of dissolved organic phosphate (DOP). Assuming biological processes are properly represented by the Redfield ratios, and that our transports are exact, this result would imply that in individual boxes about 50% of the uptake (outgassing) is consumed (produced) by DOP that was advected into (exported from) the region. In other oceanic regions, DOP effects either cancel (Southern Indian and Pacific) or reverse the net O_2 air-sea fluxes.

[38] An alternative approach to estimate the solubility pump, following *Holfort et al.* [1999], is to assign a 1500 kmol O_2 s^{-1} flux per PW (Petawatt). Our North Atlantic heat loss between 24°N and 48°N of 0.5 ± 0.1 PW [*Ganachaud and Wunsch*, 2000] would imply an uptake of 750 ± 150 kmol O_2 s^{-1}, close to the model estimate (600 ± 200 kmol O_2 s^{-1}). Conversely, the air-sea flux predicted by O* is 3 times larger at 2000 ± 500 kmol O* s^{-1}. There is a similar situation in the South Atlantic between 30°S and 45°S, with 450 ± 150 kmol O_2 s^{-1} from solubility versus 600 ± 300 kmol O_2 s^{-1} (3300 ± 1100 kmol O* s^{-1}) from the model. The reason for the discrepancy is possibly an underestimate of the solubility pump (see below), an inappropriate representation of biology by a simple Redfield ratio, or the result of a strong seasonal alias in nutrient transports that created spurious phosphate divergences (see the Discussion).

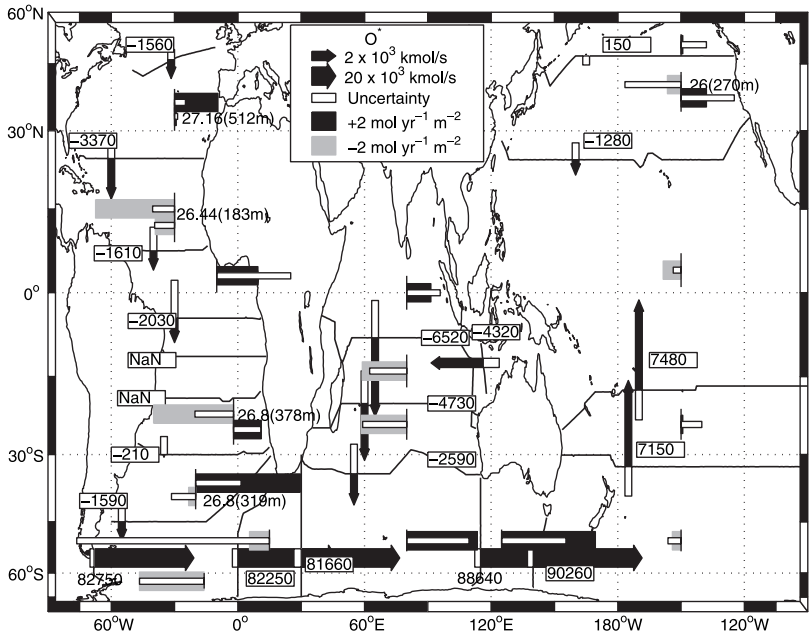

Figure 8. Same as Figure 6 but for $O^* = O + 170P$. Residual indicate net air-sea fluxes excluding biology.

[39] Zonal summations of oxygen divergences (Figure 9) reveal a source of 1050 ± 630 kmol O_2 s^{-1} in the 24°N–48°N latitude band and of 2400 ± 650 kmol O_2 s^{-1} north of 48°N. In the subtropical and tropical band (30°S–24°N), there is a sink of 6000 ± 1200 kmol O_2 s^{-1}, while in the Southern Ocean the source is of the same magnitude as the northern counterpart with 3400 ± 700 kmol O_2 s^{-1}. The global oxygen budget is in balance within the uncertainty (900 ± 1500 kmol O_2 s^{-1}). O* exhibits similar features with larger amplitudes (Figure 9), while the approximate solubility pump underestimates zonal air-sea fluxes. *Stephens et al.* [1998] compared the time-average atmospheric potential oxygen (APO = O_2 + CO_2) fluxes using ocean biological general circulation models, an atmospheric model and atmospheric observations from nine stations. Using meridional atmospheric gradients of APO, they concluded that the ocean GCMs underestimated the southward oxygen transports, resulting in a spurious uptake in the Southern Ocean. This conclusion was contradicted by *Gruber et al.* [2001] who argued that the APO gradients of *Stephens et al.* [1998] were influenced by fossil fuel emission and seasonal rectification. By inverting a global circulation model, *Gruber et al.* [2001] found, as we do, important oxygen uptake in the Southern Ocean.

5.2. Relation to Photosynthesis and Oxidation

[40] Table 4 shows previous estimates of oxygen utilization rate (OUR) and production from a variety of methods. The *Sarmiento et al.* [1990] estimate for North Atlantic OUR ranges 2.4–2.5 mol O_2 $m^{-2}yr^{-1}$, when derived from tritium inventories, and 8.5 ± 0.8 mol O_2 $m^{-2}yr^{-1}$ when derived from ^{228}Ra measurements. Those authors argue that the ^{228}Ra values are more reliable than those from the tritium inventory, although the results have not yet been supported by other techniques. Our South Atlantic O_2 loss (20°S–30°S, Figure 6) is of the same size (≃8 mol O_2 $m^{-2}yr^{-1}$), although it may include up to 50% outgassing, i.e., Figure 8. In the tropical Atlantic, our OUR estimate is lower, at 2 ± 1 mol O_2 $m^{-2}yr^{-1}$, deeper than γ^n = 26.44 (about 200 meter depth).

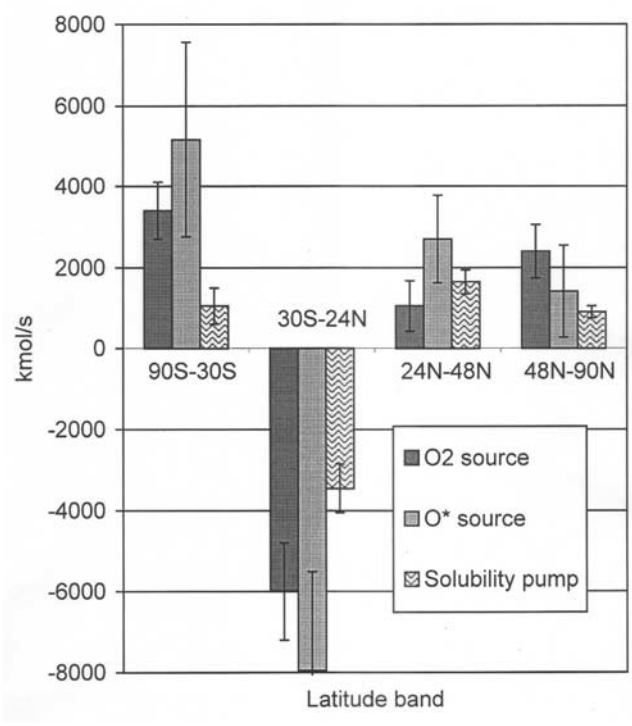

Figure 9. Global oxygen sources and sinks for selected latitude rangesform inverse model estimate for O and O* and from the estimated solubility pump (see text). Uncertainties on the later are simply 1500 × (uncertainty on heat flux) and therefore are a lower bound.

Table 4. Estimates of Oxygen Utilization Rates (OUR) and New Production[a]

Location	Method	OUR	New Production	Reference
Subtropical North Atlantic	tritium budget	2.4 to 3.5		*Sarmiento et al.* [1990]
Subtropical North Atlantic	^{228}Ra	8.5 ± 0.8		*Sarmiento et al.* [1990]
54° S–45° N	hydrographic model-based	2.5 ± 0.8		*Riley* [1951]
Sargasso Sea	tritium/^{3}He	7.2		*Jenkins* [1980]
30°N, 30° W	He age	6.4 ± 0.3		*Jenkins* [1987]
64°N, 28° W	O_2 production in mixed layer		5.2	*Peng et al.* [1987]
Near Bermuda	O_2 balance		3 to 4	*Musgrave et al.* [1988]
Near Bermuda	O_2 balance		5.6 ± 1.5	*Spitzer and Jenkins* [1989]

[a] Values are mol yr^{-1} m^{-2}. Estimates are adapted From *Sarmiento et al.* [1990].

[41] In the subtropical North Atlantic, OUR is not significantly different from zero below γ^n = 27.16 (about 500 meters, Figure 6) at 0.3 ± 0.3 mol O_2 $m^{-2}yr^{-1}$ while there is a significant uptake above that surface (1.1 ± 0.2 mol O_2 $m^{-2}yr^{-1}$), in contrast with the results of *Sarmiento et al.* [1990]. (The uncertainty is small compared with the uncertainties of the horizontal oxygen transports at 24°N and 48°N because of the correlations between errors [i.e., *Ganachaud*, 1999, p. 146].) Because most of the oxygen input occurs in regions of large oceanic cooling such as the Gulf Stream north of 36°N, at least in the GCM simulation of *Stephens et al.* [1998], *Sarmiento et al.* [1990] probably underestimate this uptake because of limited data coverage. In the North Atlantic between 24°N and 36°N, *Rintoul and Wunsch* [1991] reported a net, "barely significant", loss of oxygen of 1.3 mol O_2 $m^{-2}yr^{-1}$, which is difficult to compare with the gain that we estimate between 24°N and 48°N as the latter may be dominated by a large oxygen uptake between 36°N and 48°N. Zonal summations (Table 5) show a net, global oxygen utilization of 620 ± 320 kmol O_2 s^{-1}(0.2 ± 0.1 mol O_2 m^{-2} yr^{-1}), between 30° S and 47° N, and below 2000 m. Below the first layer, the utilization is of 4600 kmol O_2 s^{-1} (0.64 mol O_2 m^{-2} yr^{-1}) for the same area.

6. Summary and Discussion

[42] Using a geostrophic inverse box model, souces and sinks of dissolved silica, nitrate, phosphate and oxygen are estimated over large oceanic areas. This approach is complementary to numerical biogeochemical ocean models, as nutrient transport estimates are independent of assumptions about the biogeochemical behavior (usually a power law for particle dissolution [*Najjar et al.*, 1992; *Schlitzer*, 2002]). As a result, quantitative tests of biogeochemical models can be made.

[43] The vertical structure of nutrient sources and sinks, was related to export production. At shallow levels, a possible signature of time-mean, large-scale average export production is found for silica, nitrate and phosphate in several temperate regions. In individual boxes, maximum remineralization in the subsurface layers ranges between 0 ± 0.1 mol N $m^{-2}yr^{-1}$ (e.g., in the central and South Pacific) and 0.7 ± 0.25 mol N $m^{-2}yr^{-1}$ (in the South Atlantic, south of 19°S), similar to sediment trap and isotopic data.

[44] On global scales, the estimated net export is 390 ± 240 kmol Si s^{-1} and 57 ± 40 kmol N s^{-1} (420 ± 290 kmol C s^{-1}) between 47° N and 30° S, and at 2000 m. No statistically significant value could be obtained in the Southern Ocean, where all layers outcrop. The estimated values are lower by a factor of two compared to the global export rate of *Schlitzer* [2002] (130 kmol N s^{-1}, between 30°S and 50°N using his normalization) and of *Najjar et al.* [1992]. Examination of N* provides regional estimates of N fixation and denitrification that are consisten with previous findings in the North Atlantic, and contradictory in other areas such as the Indian Ocean.

[45] Because of the wide spacing between hydrographic sections, nutrient divergences can only be diagnosed over large oceanic areas enclosing varying biogeochemical regimes. As a result, our divergences may underestimate the shallow export production as classically defined, i.e., the downward flux of particles under the euphotic zone. Nevertheless, our estimate corresponds to the net quantities of nutrients that are carried to deep layers, thus excluding the part that is locally recirculated at the surface. Such estimates are of critical importance to climate studies as they correspond to carbon that is exported to deep layers, and therefore removed from the atmophere on relatively long oceanic time scales. The present estimates can be refined using similar models that include meridional sections to increase spatial resolution in specific production regimes.

[46] Despite the remaining large uncertainties, the magnitudes of the estimated large scale exports are consistent with sediment trap and isotopic data. Net sources and sinks of nutrients are found in several regions too, but all are indistinguishable from zero within a two-standard-deviation uncertainty. Imbalances may be related to advection of dissolved organic matter [*Najjar et al.*, 1992]; to aliasing of the seasonal or interannual variability in the biological activity (particle flux) and/or seasonal rectification of advective nutrient transports. Time variability in biological activity itself can introduce additional biases when estimating a time-average because of the different time scales for production and dissolution [*Deuser et al.*, 1995].

Table 5. Same as Table 1 but for Oxygen Utilization (kmol O_2 s^{-1})

	O_2 Sink Below		
Region	2000 m	1000 m	Surface
30°S–47°N	620 ± 320	1600 ± 800	4600
ATL	−70 ± 140	300 ± 240	2200 ± 600
IP	690 ± 280	1300 ± 780	2400
TROP	160 ± 250	1600 ± 800	2800
SUBP	460 ± 300	0 ± 600	1800 ± 200

[47] Oxygen utilization rates are derived from subsurface oxygen sinks and regions of important air-sea exchanges are found. Analysis of O* suggests that horizontal transports of DOP substantially affect local oxygen budgets. There is net oxygen outgassing in tropical regions and net uptake at high latitudes in both hemispheres, with a global oceanic balance for both O_2 and O^*. This distribution is consistent with independent estimates from numerical model inversions.

[48] Solubility produces air-sea exchanges of CO_2 that are similar to O_2, while biology creates exchanges that are in the opposite direction to the solubility pump for CO_2 but in the same direction for O_2. Therefore the balanced oxygen budget suggests that solubility and biological CO_2 exchanges are in global balance as well, within the estimated uncertainties. Conversely, oceanic uptake of anthropogenic CO_2 may occur as a simple partial pressure equilibration in response to atmospheric CO_2 increase, and independently of the biological and solubility pumps [e.g., *Sarmiento et al.*, 1992].

[49] By construction of the inverse model, the uncertainties that we report take into account the temporal variability in the mass, and, to some extent, advective dissolved silicate transports [*Ganachaud*, 2001]. However, variability in mass, nitrate, phosphate and oxygen transports was not fully accounted for, and is possibly underestimated, suggesting several foci for future ocean measurements. *Williams and Follows* [1998], for instance, suggest that seasonal rectification of Ekman nitrate transport is of major importance in the northern boundary of the subtropical gyre. To estimate such rectification, seasonal repeat sections in the upper water column would be necessary.

[50] We are probably close to the limits of possible accuracy in time-average flux determinations permitted by single hydrographic sections. (The fundamental, ergodic, assumption is that large areal averages represent long-time averages, and this assumption is unlikely to be completely accurate.) Regions with large oceanic variability are the main sources of remaining uncertainty. In particular, the average tracer transport through the Indonesian Throughflow is very poorly known, and its value affects the nutrient and oxygen budgets over the entire Indian and Pacific Oceans. More generally, significant improvement in the transports and divergences estimated here, is likely obtainable only through the averaging of repeated sections, some which already exist, to reduce the noise. Design of future surveys, which in the past have been essentially zonal or meridional, will also benefit from optimization by enclosing areas of high productivity or strong air-sea fluxes with hydrographic sections.

Appendix A: A Priori Silica Uncertainties

[51] The a priori uncertainties of silicate conservation equations (or, equivalently, the weight attributed to those equations) were extended globally from the *Ganachaud* [2001] North Atlantic results as follows. Mass and tracer transports are measured from a quasi-synoptic section so that any variability in temperature, salinity and silicate is aliased with respect to the time mean. Simulation of this alias based on a reconstructed silicate transport in a general circulation model suggested use of an a priori uncertainty of ±100 kmol Si s^{-1} rms in the North Atlantic Ocean, between 24°N and 36°N. To extend this result to other oceans, the following ad-hoc method was used: for a given uncertainty in the mass budget ($\Delta\text{Mass}^{\text{local}}$), it is assumed that a larger average silica concentration implies larger silicate differences over the water column and thus a larger variability in the silicate transport so that,

$$\Delta\text{Si}^{\text{local}} = \Delta\text{Si}^{\text{Reference}} \times \frac{\langle \text{Si}^{\text{local}} \rangle}{\langle \text{Si}^{\text{Reference}} \rangle} \times \frac{\Delta\text{Mass}^{\text{local}}}{\Delta\text{Mass}^{\text{Reference}}}, \qquad (2)$$

where Δ is the a priori uncertainty and $\langle \text{Si} \rangle$ is the concentration. The reference for the uncertainty in the mass and silicate conservation equations are taken in the North Atlantic mid-latitudes (respectively $\Delta\text{Mass}^{\text{Reference}} = \pm 7 \times 10^9$ kg $s^{-1}$and $\Delta\text{Si}^{\text{Reference}} = \pm 100$ kmol Si s^{-1}). Local uncertainties in the mass conservation equations ($\Delta\text{Mass}^{\text{local}}$) are function of latitude [*Ganachaud*, 2002].

[52] For practical reasons (i.e., programming issues), no constraint was imposed on the global silicate budget. Such constraint would be, to some extent, redundant with the regional silicate conservation constraints.

Table B1. Transoceanic Property Transports in kmol s^{-1}[a]

Latitude	Silica	Nitrate	Phosphate	Oxygen
ATL 47N	−130 ± 50	10 ± 35	1.1 ± 2.5	−1750 ± 500
ATL 24N	−220 ± 80	−50 ± 50	−7.6 ± 3.6	−2070 ± 600
ATL 7.5N	−160 ± 110	−70 ± 120	−1.0 ± 7	−1430 ± 950
ATL 4.5S	−190 ± 170	−210 ± 150	−11 ± 10	−140 ± 1570
ATL 11S	−230 ± 154	−180 ± 140	*N/A*	−1380 ± 1250
ATL 19S	−130 ± 107	−60 ± 80	*N/A*	−1590 ± 700
ATL 30S	−180 ± 140	−70 ± 80	−4 ± 5	430 ± 680
ATL 45S	−110 ± 190	−240 ± 90	−9 ± 6	−50 ± 710
Drake	9720 ± 880	4340 ± 190	302 ± 13	31380 ± 1230
S.O. 0E	9810 ± 900	4300 ± 250	295 ± 17	32170 ± 1900
S.O. 30E	9810 ± 920	4090 ± 340	295 ± 27	31550 ± 1900
S.O. 115E	9550 ± 920	4620 ± 260	320 ± 18	34250 ± 1840
S.O. 140E	9530 ± 920	4700 ± 270	329 ± 18	34350 ± 1800
PAC 32S	−250 ± 380	190 ± 136	14 ± 10	4730 ± 1000
PAC 17S	−110 ± 420	270 ± 170	25 ± 12	3260 ± 1100
PAC 24N	40 ± 340	−10 ± 100	0 ± 8	−1300 ± 680
PAC 47N	70 ± 150	80 ± 40	5 ± 3	−670 ± 450
ITF[b]	−390 ± 190	−160 ± 80	−12 ± 6	−2250 ± 410
IND 32S	240 ± 380	−90 ± 130	−4 ± 9	−1820 ± 1090
IND 19S	20 ± 440	−240 ± 150	−19 ± 10	−1430 ± 1210
IND 8S	−270 ± 530	−410 ± 210	−28 ± 15	−1770 ± 1750

[a] Positive is northward or eastward; uncertainties are one standard deviation.

[b] We believe that Indonesian Throughflow (ITF) uncertainty is twice the formal uncertainty reported here. See *Ganachaud et al.* [2000].

Appendix B: Tracer Transports and Divergences

[53] Tables B1 and B2 show the net transports and divergences associated with the circulation.

[54] **Acknowledgments.** This work was completed while A. G. was graduate student in the MIT/WHOI Joint Program in Physical Oceanography and benefited from the advice of D. Glover, J. Toole, B. Warren, J. Marotzke, and N. Hogg. At the early stage of this study, W. Jenkins' expertise was appreciated. Conversations and comments from P. Tréguer, M. Follows and G. McKinley contributed to improve the manuscript. The

Table B2. Sources and Sinks in kmol s^{-1}[a]

Between and Next[b]	Silica	Nitrate	N*	Phosphate	Oxygen	O*
ATL 47N	80 ± 70	50 ± 40	−77 ± 20	8 ± 3	590 ± 210	1930 ± 470
ATL 24N	−66 ± 100	10 ± 130	110 ± 40	−8 ± 8	−1920 ± 500	−3200 ± 1030
ATL 7.5N	−64 ± 160	110 ± 220	−6 ± 50	8 ± 13	−510 ± 1020	920 ± 1660
ATL 4.5S	80 ± 190	N/A	N/A	N/A	650 ± 1010	N/A
ATL 11S	−50 ± 130	−110 ± 130	N/A	N/A	520 ± 650	N/A
ATL 19S	60 ± 90	66 ± 80	−20 ± 35	5 ± 5	−2000 ± 260	−1110 ± 820
ATL 30S	90 ± 160	250 ± 100	90 ± 40	10 ± 6	610 ± 310	2310 ± 1140
45S/Dk[c]	−10 ± 400	−270 ± 160	−10 ± 90	−16 ± 10	740 ± 920	−2040 ± 2040
S.O. 0E	20 ± 400	−200 ± 270	−215 ± 245	0 ± 20	−550 ± 1040	−430 ± 4160
30E/I5[d]	10 ± 480	450 ± 280	100 ± 240	20 ± 20	1010 ± 910	4660 ± 4110
S.O. 115E	−20 ± 360	90 ± 100	−60 ± 35	10 ± 6	130 ± 570	1700 ± 1170
140E/Dk	−130 ± 550	−210 ± 140	30 ± 60	−15 ± 10	1510 ± 650	−1050 ± 1580
PAC 32S	80 ± 270	60 ± 130	−90 ± 26	9 ± 9	−1440 ± 580	115 ± 1335
17S/ITF[e]	700 ± 360	−60 ± 160	70 ± 40	−8 ± 11	−2070 ± 750	−3460 ± 1510
PAC 24N	−70 ± 370	50 ± 110	20 ± 30	2 ± 8	460 ± 590	770 ± 960
PAC 47N						
IND 32S	−110 ± 280	−120 ± 130	80 ± 40	−12 ± 8	710 ± 410	−1390 ± 1350
IND 19S	−310 ± 320	−230 ± 130	−30 ± 20	−13 ± 9	910 ± 730	−1280 ± 1070
IND 8S	−140 ± 490	240 ± 210	2 ± 30	15 ± 14%	−1220 ± 1060	1260 ± 1750
ITF						

[a] Sources and sinks are calculated from the sum of the divergences of property transports (horizontal and vertical) within each individual layers of the model and may differ from differences between net transports. Because they imply strict mass conservation, divergences of anomalies are believed to be more accurate. Positive is a source; negative is a sink.

[b] The source (positive) or sink (negative) is given between the section indicated and the one in the next row.

[c] Drake.

[d] IND 32S.

[e] Indonesian Throughflow.

authors are grateful to the Principal Investigators who provided the data from the World Ocean Circulation Experiment and the Franco-Indonesian Java-Australia Dynamic Experiment. Supported by Jet Propulsion Laboratory Contract No. 958125; by gifts from Ford, General Motors, and Daimler-Chrysler to MIT's Climate Modelling Initiative; and by the Centre National d'Etudes Spatiales. Contribution to the World Ocean Circulation Experiment.

References

Anderson, L. A., and J. L. Sarmiento, Redfield ratios of remineralization determined by nutrient data analysis, *Global Biogeochem. Cycles*, *8*(1), 65–85, 1994.

Antoine, D., J.-M. André, and A. Morel, Oceanic primary production, 2, Estimation at global scale from satellite chlorophyll, *Global Biogeochem. Cycles*, *10*(1), 57–69, 1996.

Archer, D., M. Lyle, K. Rodgers, and P. Frolich, What controls opal preservation in tropical deep-sea sediments?, *Paleoceanography*, *8*(1), 7–21, 1993.

Aufdenkampe, A., J. McCarthy, M. Rodier, C. Navarette, J. Dunne, and J. Murray, Estimation of new production in the tropical Pacific, *Global Biogeochem. Cycles*, *15*, 101–112, 2001.

Broecker, W. S., and T.-H. Peng, *Tracers in the Sea*, 690 pp., Lamont-Doherty Earth Obs., Palisades, N. Y., 1982.

Buesseler, K. O., Do upper-ocean sediment traps provide an accurate record of particle flux?, *Nature*, *353*, 420–423, 1991.

Buesseler, K. O., The decoupling of production and particulate export in the surface ocean, *Global Biogeochem. Cycles*, *12*(2), 297–310, 1998.

DeMaster, D. J., T. M. Nelson, S. L. Harden, and C. A. Nittrouer, The cycling and accumulation of biogenic silica and organic carbon in Antarctic deep-sea and continental margin environments, *Mar. Chem.*, *35*, 489–502, 1991.

Deuser, W. G., T. D. Jickells, P. King, and J. A. Commeau, Decadal and annual changes in biogenic opal and carbonate fluxes in the deep Sargasso Sea, *Deep Sea Res., Part I*, *42*(11/12), 1923–1932, 1995.

Deutsch, C., N. Gruber, R. M. Key, and J. L. Sarmiento, Denitrification and N_2 fixation in the Pacific Ocean, *Global Biogeochem. Cycles*, *15*, 483–506, 2001.

Ganachaud, A., Large scale oceanic circulation and fluxes of freshwater, heat, nutrients and oxygen, Ph.D. thesis, 267 pp., Mass. Inst. of Technol./Woods Hole Oceanogr. Inst. Joint Program, Cambridge, Mass., 1999.

Ganachaud, A., and C. Wunsch, The oceanic meridional overturning circulation, mixing, bottom water formation and heat transport, *Nature*, *408*, 453–457, 2000.

Ganachaud, A., C. Wunsch, J. Marotzke, and J. Toole, The meridional overturning and large-scale circulation of the Indian Ocean, *J. Geophys. Res.*, *105*, 26,117–26,134, 2000.

Garcia, H. E., and L. I. Gordon, Oxygen solubility in seawater: Better fitting equations, *Limnol. Oceanogr.*, *37*(6), 1307–1312, 1992.

Gordon, A. L., R. D. Susanto, and A. Ffield, Throughflow within the Makassar Strait, *Geophys. Res. Lett.*, *26*, 3325–3328, 1999.

Gruber, N., and J. Sarmiento, Global patterns of marine nitrogen fixation and denitrification, *Global Biogeochem. Cycles*, *11*, 235–266, 1997.

Gruber, N., E. Gloor, S.-M. Fan, and J. L. Sarmiento, Air-sea flux of oxygen estimated from bulk data: Implications for the marine and atmospheric oxygen cycles, *Global Biogeochem. Cycles*, *15*, 783–803, 2001.

Holfort, J., K. M. Johnson, B. Schneider, G. Siedler, and D. W. R. Wallace, Meridional transport of dissolved inorganic carbon in the South Atlantic Ocean, *Global Biogeochem. Cycles*, *13*(1), 253–254, 1999.

Jackett, D. R., and T. J. McDougall, A neutral density variable for the world's oceans, *J. Phys. Oceanogr.*, *27*, 237–263, 1997.

Jenkins, W. J., Tritium and ^{3}He in the Sargasso Sea, *J. Mar. Res.*, *38*, 533–569, 1980.

Jenkins, W. J., ^{3}H and ^{3}He in the Beta Triangle: Observations of gyre ventilation and oxygen utilization rates, *J. Phys. Oceanogr.*, *17*, 763–781, 1987.

Jenkins, W., and J. Goldman, Seasonal cycling and primary production in the Sargasso Sea, *J. Mar. Res.*, *43*, 465–491, 1985.

Keeling, R. F., and T.-H. Peng, Transport of heat, CO_2 and O_2 by the Atlantic's thermohaline circulation, *Philos. Trans. R. Soc. London, Ser. B*, *348*, 133–142, 1995.

Lampitt, R. S., and A. N. Antia, Particle flux in deep seas: Regional characteristics and temporal variability, *Deep Sea Res., Part I*, *44*(8), 1377–1403, 1997.

Laws, E. A., P. G. Falkowski, W. O. Smith, H. Ducklow, and J. J. McCarthy, Temperature effects on export production in the open ocean, *Global Biogeochem. Cycles*, *14*, 1231–1246, 2000.

Macdonald, A., The global ocean circulation: A hydrographic estimate and regional analysis, *Prog. Oceanogr.*, *41*, 281–382, 1998.

McKinley, G. A., M. Follows, and J. Marshall, Interannual variability of the air-sea flux of oxygen in the North Atlantic, *Geophys. Res. Lett.*, *27*, 2933–2936, 2000.

Michaels, A. F., N. R. Bates, K. O. Buesseler, C. A. Carlson, and A. H. Knap, Carbon-cycle imbalances in the Sargasso Sea, *Nature*, *372*, 537–540, 1994.

Musgrave, D. L., J. Chou, and W. J. Jenkins, Application of a model of upper-ocean physics for studying seasonal cycles of oxygen, *J. Geophys. Res.*, *93*, 15,679–15,700, 1988.

Najjar, R., J. Sarmiento, and J. Toggweiler, Downward transport and fate of organic matter in the ocean: Simulations with a general circulation model, *Global Biogeochem. Cycles*, *6*, 45–76, 1992.

Nelson, D. M., P. Tréguer, M. A. Brezezinski, A. Leynaert, and B. Queguiner, Production and dissolution of biogenic silica in the ocean: Revised global estimates, comparison with regional data and relationship to biogenic sedimentation, *Global Biogeochem. Cycles*, *9*, 359–372, 1995.

Peng, T.-H., T. Takahashi, and W. S. Broecker, Seasonal variability of carbon dioxide, nutrients and oxygen in the northern North Atlantic surface water: Observations and a model, *Tellus, Ser. B*, *39*, 439–458, 1987.

Ragueneau, O., et al., A review of the Si cycle in the modern ocean: Recent progress and missing gaps in the application of biogenic opal as a paleoproductivity proxy, *Global Planet. Change*, *26*, 317–365, 2000.

Riley, G. A., Oxygen, phosphate and nitrate in the Atlantic Ocean, *Bull. Bingham Oceanogr. Coll.*, *12*, 169 pp., 1951.

Rintoul, S. R., and C. Wunsch, Mass, heat, oxygen and nutrient fluxes and budget in the North Atlantic Ocean, *Deep Sea Res*, *38*, 355–377, 1991.

Sarmiento, J. L., G. Thiele, R. M. Key, and W. S. Moore, Oxygen and nitrate new production and remineralization in the North-Atlantic subtropical gyre, *J. Geophys. Res.*, *95*, 18,303–18,315, 1990.

Sarmiento, J. L., J. C. Orr, and U. Siegenthaler, A perturbation simulation of CO_2 uptake in an ocean general circulation model, *J. Geophys. Res.*, *97*, 3621–3645, 1992.

Sayles, F. L., W. G. Deuser, J. E. Goudreau, W. H. Dickinson, T. D. Jickells, and P. King, The benthic cycle of biogenic opal at the Bermuda Atlantic Time Series site, *Deep Sea*, 1–27, 1996.

Schlitzer, R., Carbon export fluxes in the Southern Ocean: Results from inverse modeling and comparison with satellite based estimates, *Deep Sea Res., Part II*, *49*, 1623–1644, 2002.

Siegel, D. A., and W. G. Deuser, Trajectories of sinking particles in the Sargasso Sea: Modelling of statistical funnels above deep-ocean sediment traps, *Deep Sea Res., Part I*, *44*, 1519–1541, 1997.

Spitzer, W. S., and W. J. Jenkins, Rates of vertical mixing, gas exchange and new production: Estimates from seasonal gas cycles in the upper ocean near Bermuda, *J. Mar. Res.*, *47*, 169–196, 1989.

Stephens, B. B., R. F. Keeling, M. Heimann, K. D. Six, R. Murnane, and K. Caldeira, Testing global ocean carbon cycle models using measurements of atmospheric O_2 and CO_2 concentration, *Global Biogeochem. Cycles*, *12*, 213–230, 1998.

Tréguer, P., D. M. Nelson, A. J. van Bennekom, D. J. DeMaster, A. Leynaert, and B. Quéguiner, The silica balance in the World Ocean: A reestimate, *Science*, *268*, 375–379, 1995.

Williams, R. G., and M. J. Follows, The Ekman transfer of nutrients and maintenamce of new production over the North Atlantic, *Deep Sea Res., Part I*, *45*, 461–489, 1998.

Wunsch, C., *The Ocean Circulation Inverse Problem*, 437 pp., Cambridge Univ. Press., New York, 1996.

A. Ganachaud, Institut de Recherche pour le Developpement, Centre de Noumea, BP A5 Noumea, New Caledonia. (alexandre.ganachaud@noumea.ird.nc)

C. Wunsch, Massachusetts Institute of Technology, 77 Massachusetts Avenue, Cambridge, MA 02139, USA.